J Mater Sci (2014) 49:6517–6528
DOI 10.1007/s10853-014-8203-6

ULTRAFINEGRAINED MATERIALS

Effect of anvil roughness on the flow patterns and hardness development in high-pressure torsion

Yi Huang · Megumi Kawasaki · Ahmed Al-Zubaydi · Terence G. Langdon

Received: 31 January 2014 / Accepted: 26 March 2014 / Published online: 16 April 2014

Abstract Two sets of anvils having different surface roughness were used to systematically investigate the flow patterns developed on the top and bottom surfaces of stainless steel discs with an anvil misalignment of 100 μm during high-pressure torsion. It is shown that the flow patterns on the disc surfaces have different variation tendencies depending on whether the anvils have rough or smooth surfaces. Double-swirl flow patterns were observed on the top and bottom surfaces of discs after 1 and 5 turns when using an anvil with a smooth surface. In contrast, when using an anvil with a rough surface the double-swirl flow patterns appeared only on the top surface after 1 turn and a single swirl appeared on both surfaces after 5 turns. Hardness measurements on the top surfaces showed that discs processed using an anvil with a rough surface have greater hardness than discs processed using an anvil with a smooth surface. There was no obvious hardness difference on the bottom surfaces for discs processed using anvils with rough or smooth surfaces.

Y. Huang (✉) · A. Al-Zubaydi · T. G. Langdon
Materials Research Group, Faculty of Engineering and the Environment, University of Southampton, Southampton SO17 1BJ, UK
e-mail: y.huang@soton.ac.uk

M. Kawasaki · T. G. Langdon
Departments of Aerospace & Mechanical Engineering and Materials Science, University of Southern California, Los Angeles, CA 90089-1453, USA

M. Kawasaki
Division of Materials Science and Engineering, Hanyang University, 17 Haengdang-dong, Seongdong-gu, Seoul 133-791, South Korea

Introduction

High-pressure torsion (HPT) is a mature severe plastic deformation technique which is regularly used to achieve significant grain refinement [1]. There are many published results on HPT processing of various metals and alloys [2] and recently HPT techniques were applied to the processing of metal powders [3, 4] and machining chips [5]. The uses of HPT also include mechanical mixing [6], investigations of amorphization [7, 8] and phase transformations [9–11], evaluations of the hydrogen storage capabilities of magnesium [12, 13], and examinations of the structural modifications and the mechanical properties of bulk metallic glasses [14, 15].

In the idealized HPT process, the deformation procedure can be considered as a simple shear process (rigid-body analysis) where the shear strain, γ, is evaluated using the equation [16]:

$$\gamma = \frac{2\pi Nr}{h} \tag{1}$$

where r and h are the radius and height (or thickness) of the disc, respectively, and N is the number of revolutions. In the idealized unconstrained HPT, the disc is placed between two flat anvils and the lateral flow of the material is not restricted under the applied pressure. However, this unconstrained HPT is technically difficult to implement as there is a continuous decrease in the sample thickness. In constrained HPT, the disc is placed within a cavity in the lower anvil so that the lateral flow of the material is totally restricted under the applied hydrostatic pressure. In this condition, the specimen deforms under torsional straining and under the imposed hydrostatic pressure without changes in the geometry if there is no friction force at the outer cylinder wall. However, because friction is unavoidable, a

homogenous shear deformation process cannot occur in constrained HPT. In practice, quasi-constrained HPT can overcome the drawbacks and problems associated with idealized unconstrained and constrained HPT. Most HPT processing is now conducted under quasi-constrained conditions where the disc is contained within shallow depressions on the lower and upper anvils, and there is some limited outflow of material between the two anvils during the straining operation [17, 18].

It follows from Eq. (1) that the shear strain should increase linearly with the radius of the disc. Therefore, based on the rigid-body assumption in Eq. (1), it is reasonable to anticipate that the microstructure and mechanical properties remain inhomogeneous across the disc. However, there is an additional strain on the HPT disc due to the applied compressive stress introduced in quasi-constrained HPT processing and this is not considered in Eq. (1). In practice, there is an evolution towards microstructural homogeneity in HPT and this has been effectively predicted by making use of strain gradient plasticity modelling [19]. In fact, a fully homogeneous microstructure and mechanical properties have been reported in many materials after HPT processing [13, 20–25].

Some recent experiments were conducted on a duplex stainless steel to observe visual displays of the flow patterns produced by the HPT processing [26–28]. The results were unexpected because there was evidence for the formation of significant local turbulence including the presence of double-swirl patterns and local shear strain vortices. Furthermore, double-swirl flow patterns were also observed in a Cu-28 % Ag alloy after HPT processing [29]. It is possible that the presence of double-swirl flow patterns may arise in HPT discs from a misalignment of the axes of the anvils prior to conducting the HPT processing. However, no specific information on the initial anvil alignment was available in these earlier reports, and no checks were undertaken to determine whether the anvils were in alignment [26–29]. Therefore, it is not possible to obtain a correlation between the appearance of double-swirl patterns on the disc surfaces and the inherent anvil misalignments.

The effect of a misalignment of the axes of the anvils was first considered in several reports of HPT in order to explain the reasons for attaining a fully-homogenized microstructure and hardness distribution [30, 31] but this possibility was never examined experimentally. Recently, a series of experiments were conducted to investigate the effect of different amounts of anvil misalignment on the flow patterns and hardness distributions on the top surfaces of discs in HPT processing [32–34]. These experiments showed that the presence of double-swirls on the disc top surfaces was a feature of HPT processing when the anvils had a small initial lateral misalignment.

Friction is an important factor which is needed in order to achieve the torsional straining. Therefore, the anvil surfaces are generally initially treated by sandblasting or spark erosion in order to generate a distinctive surface micro-roughness. Through this surface roughness, combined with the hydrostatic pressure, it is feasible to develop the high frictional forces that are required for rotational straining. To date, there has been no investigation to determine whether the initial anvil surface roughness has any effect on the flow patterns and the hardness distributions. Accordingly, the present research was initiated to investigate the influence of the anvil roughness on the flow patterns generated on both the top and bottom surfaces of the discs when processing by HPT.

Experimental material and procedures

A commercial F53 super duplex stainless steel was received in the form of a rolled plate having a thickness of 3 mm. This material was supplied by Castle Metals UK Ltd. (Blackburn, Lancashire. UK), and has a high yield strength up to ~570 MPa, good ductility and outstanding corrosion resistance. The chemical composition of the as-received material is given in Table 1 and the microstructure is shown in Fig. 1. The material consists of essentially equal proportions, and similar volume fractions, of the lighter-contrast austenitic (γ) and the darker-contrast ferritic (α) phases. The widths of these two phases varied between ~5 and ~50 μm.

Discs having diameters of 9.8 mm and thicknesses of ~1.2 mm were cut from the steel plate, and then ground to a uniform thickness of ~0.82 mm. The HPT processing was conducted at room temperature under quasi-constrained conditions [17, 18] using two massive anvils each machined with a central depression having a diameter of 10 mm and a depth of 0.25 mm. The term anvil misalignment is used to denote a parallel displacement of the rotation axis of the upper anvil with respect to the lower anvil, and the basic principles of anvil alignment were given in earlier reports [32–34]. In the present experiments, the anvils were set up with an initial misalignment of 100 μm.

Table 1 Chemical composition of the super duplex stainless steel

Element	C	Cr	Mn	Mo	N	Ni	P	S	Si
wt. (%)	<0.030	24.0–26.0	<1.20	3.0–5.0	0.24–0.32	6.0–8.0	<0.035	<0.020	<0.8

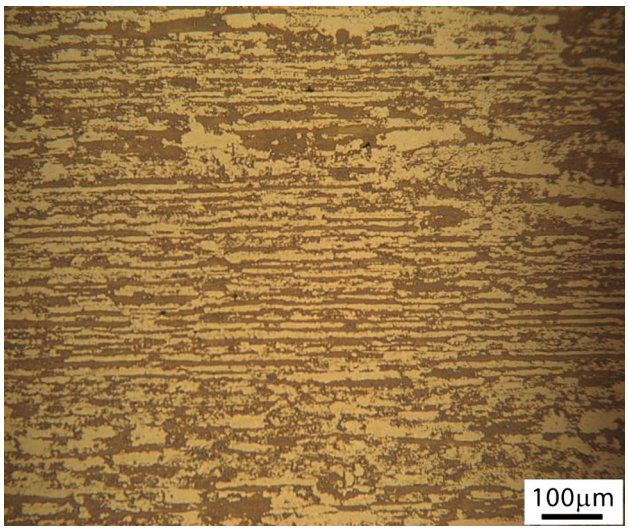

Fig. 1 Microstructure of the as-received duplex stainless steel

The surface roughness of the anvils was measured using Alicona Infinite Focus. Two sets of anvils having different surface roughness were used to investigate the flow patterns on the disc top and bottom surfaces after HPT. Figure 2 shows the anvil surface profile measurements on the two anvils which are nominally designated (a) smooth and (b) rough. For each anvil, the upper image is the anvil surface morphology as represented by a set of unique colours shown by the colour key on the right, and the lower image is the result of surface roughness measurements along the anvil surface shown in the upper image. The measured average surface roughness values of the smooth and rough anvils, R_a, were equal to 5 and 15 μm, respectively. Henceforth, these initial anvil surface conditions are named smooth with $R_a = 5$ μm and rough with $R_a = 15$ μm.

A set of discs was prepared for both of these anvil surface conditions with the discs processed at room temperature with a pressure 6.0 GPa and a rotation speed of 1 rpm through totals of $N = 1$ and 5 turns. To avoid any problems with slippage, all of the HPT processing was conducted using new anvils so that the surfaces within the depressions were in perfect condition. In addition, and following standard practice [35], some preliminary tests were conducted using discs with marker lines scribed on the top and bottom surfaces and these tests revealed no evidence for any slippage under the present experimental conditions.

After processing through 1 and 5 turns, the discs were mounted in bakelite for top and bottom surface observations. The mounted samples were mechanically polished, and then electro-etched using an electrolyte of 40 % NaOH solution at 25 °C. After etching, the γ-phase appeared bright and the α-phase appeared dark. The local flow patterns were examined using an Olympus BX51 microscope.

The values of the Vickers microhardness, Hv, were measured on the polished surfaces with separations of 0.3 mm between each consecutive point along the disc diameter. An FM300 hardness tester equipped with a Vickers indenter was used with a load of 300 gf and a dwell time of 15 s.

Experimental results

Flow pattern observations on disc top and bottom surfaces using the smooth anvil

Figure 3 shows the flow patterns developed on the disc top surface when using smooth anvils where the rows of black dots correspond to the marks from the hardness mapping indentations. The appearance of the disc top surface shows a clearly defined curvature of the phase domains for both 1 turn in Fig. 3 (a) and 5 turns in Fig. 3 (b). Close inspection shows there are pairs of curvatures for both conditions and these pairs correspond to double-swirls with each swirl having a unique swirl centre. Earlier reports demonstrated similar observations, and it was found that the double-swirl configurations decrease in size with increasing numbers of turns on the disc top surface [32–34].

Figure 4 displays the flow patterns on the disc bottom surface when using smooth anvils for (a) 1 turn and (b) 5 turns. The bottom surfaces also display well-defined curvature of the phase domains for both 1 and 5 turns. It is obvious that there are double-swirl flow patterns on the bottom surfaces and the distance between the two swirl centres is reduced with increasing numbers of rotations. The current observations on the disc bottom surfaces are different from those reported earlier where no double-swirls patterns were visible at the bottom [28]. However, the present observations are for samples processed with smooth anvils and with a measured anvil misalignment of 100 μm, whereas no information is available on either the smoothness of the anvils or the extent of the initial anvil misalignment in the earlier report.

Ideally, the flow patterns on the disc top and bottom surfaces should be identical but with the flow visible in opposite directions. Figs. 3 and 4 demonstrate this ideal symmetry because both top and bottom surfaces show the appearance of double-swirls and, as the numbers of rotations increase from 1 to 5 turns, the configuration size of the double-swirls becomes smaller on both the top and bottom surfaces.

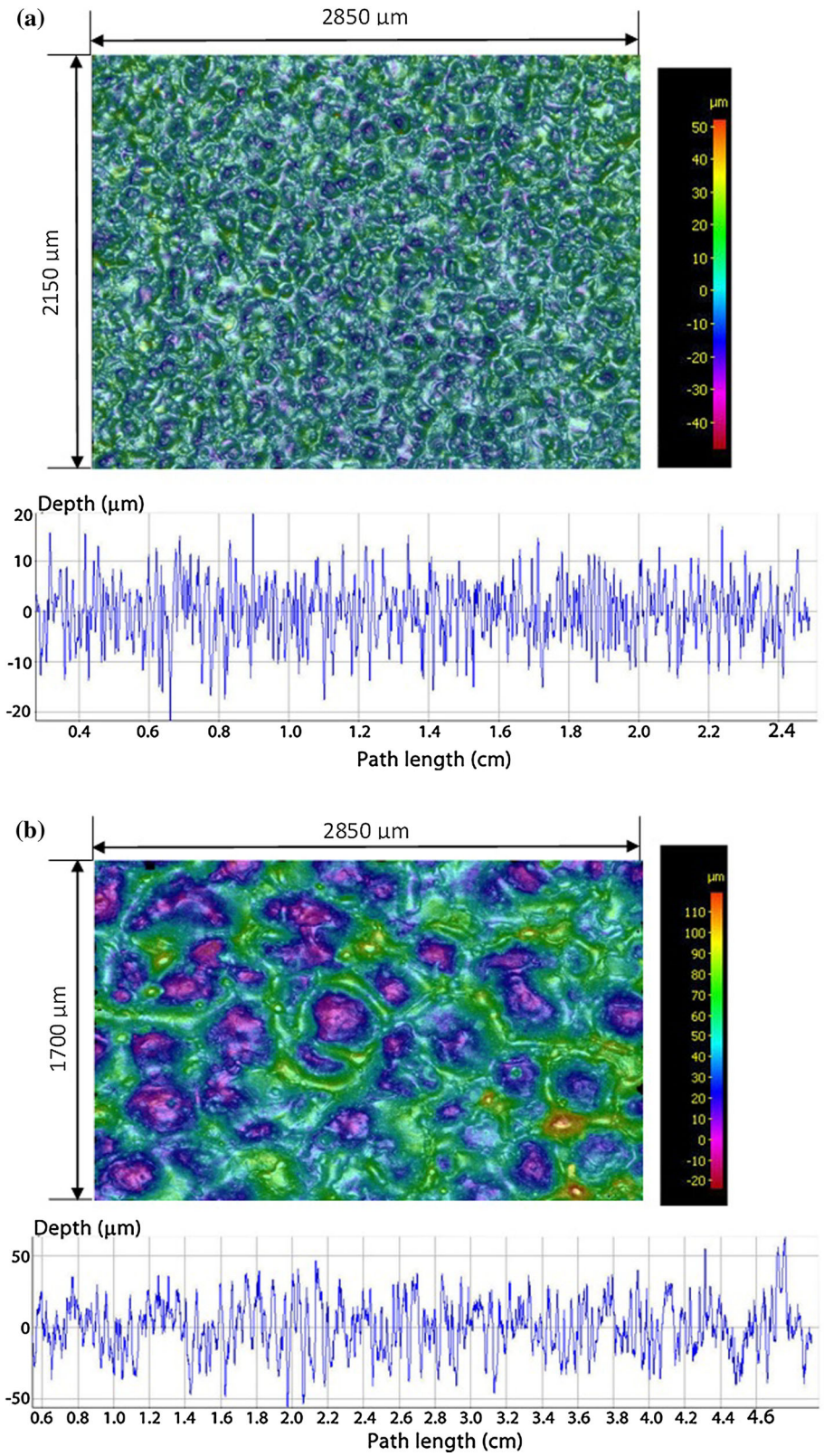

Fig. 2 Anvil surface profile measurements on **a** the smooth anvil and **b** the rough anvil: for each anvil, the *upper image* shows the surface morphology with the colour key on the right and the *lower image* shows the measurements of the surface roughness taken on the anvil surface shown in the upper image

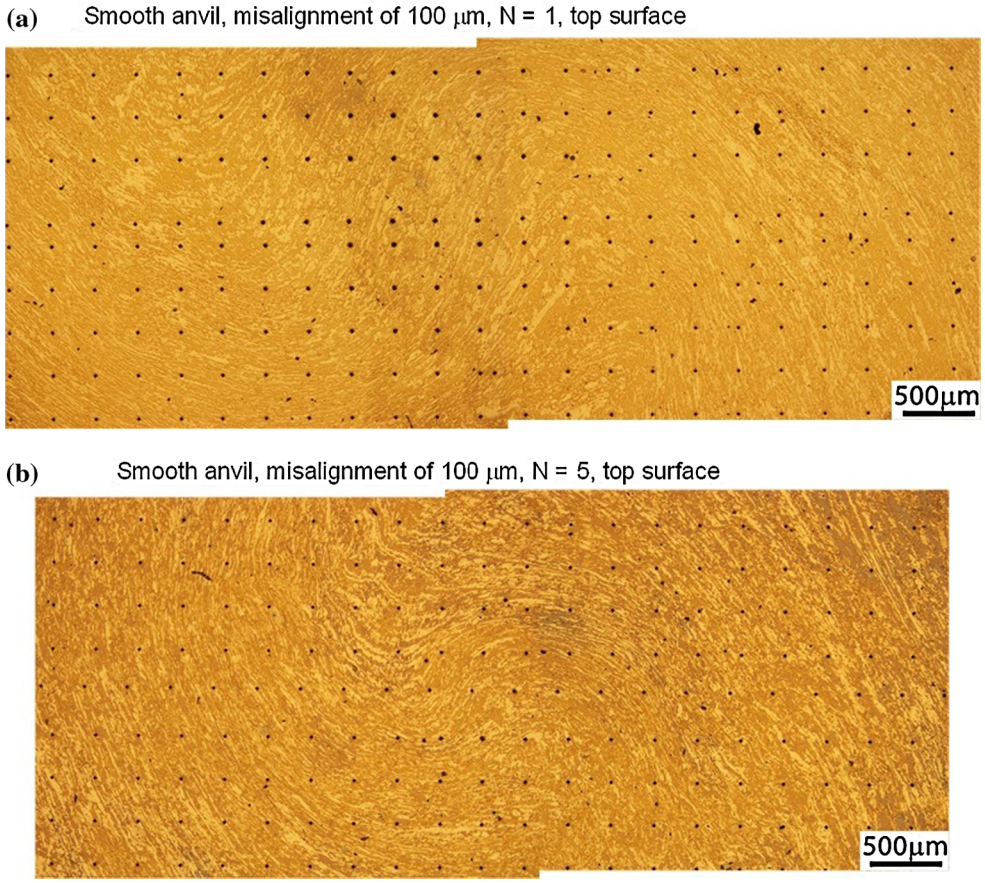

Fig. 3 The flow pattern appearance on the disc top surface while using smooth anvils ($R_a = 5$ μm) with an anvil misalignment of 100 μm for **a** $N = 1$ turn and **b** $N = 5$ turns

Flow pattern observations on disc top and bottom surfaces using the rough anvil

Figure 5 shows the flow patterns developed on the disc top surfaces when using the rough anvils. In Fig. 5 (a) and (b), the top row shows low magnification images of the phase domains along the disc diameter and the two lower rows show high magnification images of the areas in the red squares in the upper images. From the top row image in Fig. 5 (a), a double-swirl flow pattern can be recognised on the disc top surface after 1 turn, but the double-swirl is not clearly defined as on the top surface when using smooth anvils in Fig. 3 (a). Thus, in Fig. 3 (a) the austenitic (γ) and the ferritic (α) phases are clearly distinguished and the curvature of the phase domains is smooth, whereas in the top image in Fig. 5 (a) the overall curvature of the phase domains is not smooth so that some areas show clear two phase contrast and other areas display unclear phase contrast. The bottom images corresponding to the areas marked with the red squares in the top row show that the left red square contains many local vortices, whereas the right red square, which is an area showing unclear two phase contrast at the low magnification, has two phases with the widths of the austenitic (γ) and the ferritic (α) phases reduced significantly.

These observations suggest that local deformation, such as local vortices and local variations in the widths of the austenitic (γ) and ferritic (α) phase refinement, leads to a non-uniform appearance for the phase domains. After 5 turns, the disc top surface shows an overall single swirl appearance in the top row image in Fig. 5 (b). There appears to be a clear phase contrast and some local vortices, but the magnified image of the red square of the single swirl area shows that the widths of the austenitic (γ) and the ferritic (α) phases are significantly refined. Again, these observations confirm the occurrence of non-uniform deformation on the disc top surface.

The appearance of the flow patterns on the disc bottom surfaces when using a rough anvil is shown in Fig. 6 after (a) 1 turn and (b) 5 turns. After 1 turn, the domains for the austenitic γ and ferritic α phases are easily recognised in Fig. 6 (a) and the phase domains remain reasonably straight in the centres of the discs with an appearance that is generally similar to the initial as-received material shown in Fig. 1. These straight patterns continued throughout the disc bottom surface except for small

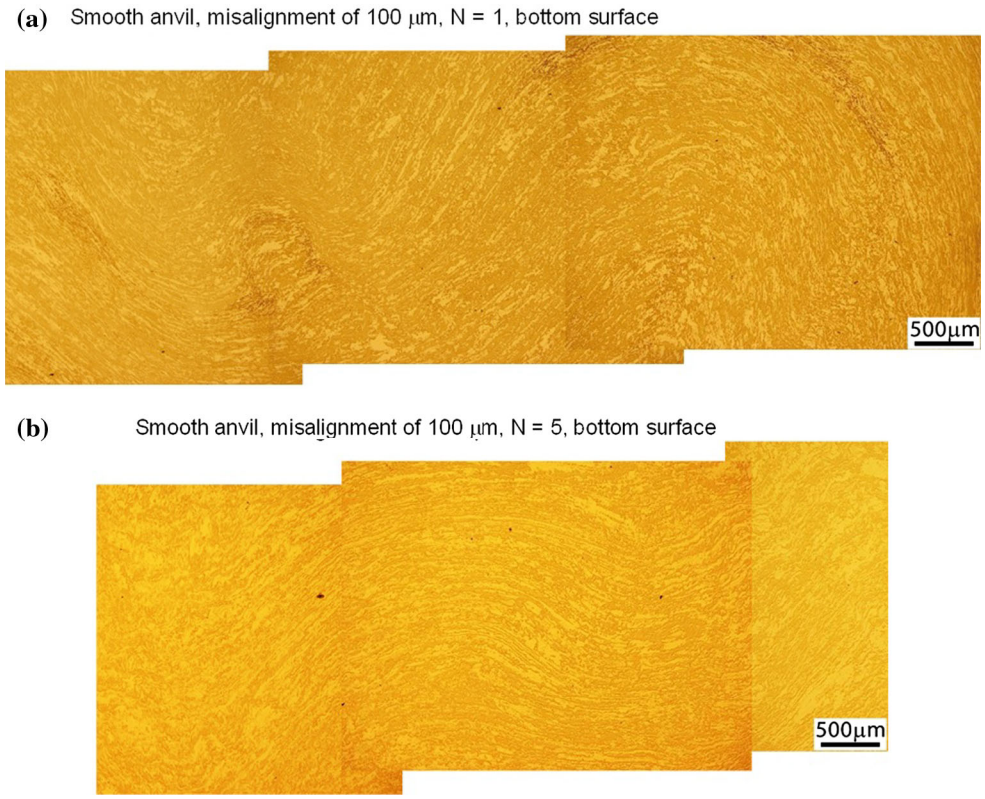

Fig. 4 The flow pattern appearance on the disc bottom surface, while using smooth anvils ($R_a = 5$ μm) with an anvil misalignment of 100 μm for **a** $N = 1$ turn and **b** $N = 5$ turns

deviations at the edges of the discs. In Fig. 6 (b), the top row shows low magnification images of the phase domains along the disc diameter and the bottom row shows high magnification images of the areas contained within the red squares in the upper images. A single swirl is clearly identified on the disc bottom surface after 5 turns as shown in the top row image of Fig. 6 (b) but in the right red square the domains of the austenitic γ and ferritic α phases cannot be identified clearly and this is similar to the single swirl observed on the disc top surface with the rough anvil after 5 turns as shown in Fig. 5 (b). The high magnification images in the bottom row of Fig. 6 (b) show the refined austenitic (γ) and the ferritic (α) phases in the right red square area and local vortices that have developed in the left red square area.

It is concluded from these observations that a rough anvil in HPT leads to different flow patterns on the disc top and bottom surfaces after 1 turn. Thus, the disc top surface shows double-swirl flow patterns in Fig. 5 (a), whereas the disc bottom surface displays straight phase domains in Fig. 6 (a). Figures 5 (b) and 6 (b) demonstrate the occurrence of ideal symmetry on the top and bottom surfaces after 5 turns because these surfaces show the same single swirl flow pattern.

A comparison of hardness evolution on the top surfaces with smooth and rough anvils

To compare the influence of smooth and rough anvils on the mechanical characteristics of the top surfaces, the hardness distributions were recorded after 1 and 5 turns as presented in Fig. 7 for (a) 1 and (b) 5 turns.

After 1 turn, the use of smooth anvils introduces double-swirl flow patterns on the disc top surface, whereas rough anvils lead to the appearance of double-swirls with non-uniform phase domain contrast. As shown in Fig. 7 (a), the hardness values on the top surface using the rough anvil are larger than with the smooth anvil. Nevertheless, the hardness distributions from the smooth and rough anvils display similar variations across the discs with a minimum hardness in the centre, higher values towards the edges and with evidence for a saturation condition at the edge of the disc over an outer ring having a width of about 2 mm.

After 5 turns, the smooth anvil generates double-swirl flow patterns on the top surface, whereas the rough anvil produces the appearance of a single swirl with a non-uniform phase domain contrast in the swirl area. In Fig. 7 (b)

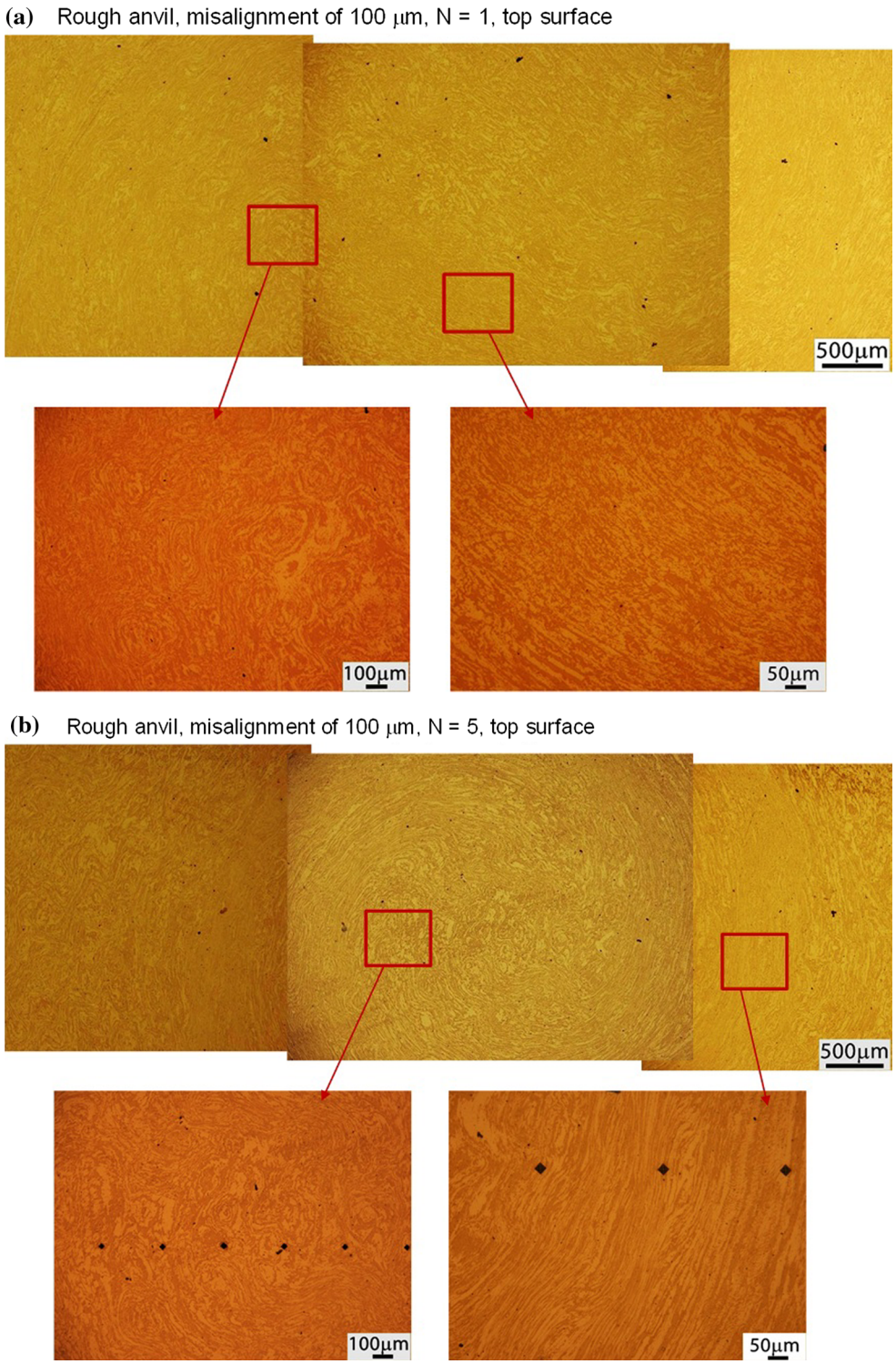

Fig. 5 The flow pattern appearance on the disc top surface while using rough anvils ($R_a = 15$ μm) with an anvil misalignment of 100 μm for **a** $N = 1$ turn and **b** $N = 5$ turns

the microhardness values after 5 turns are again larger for the rough anvil. Furthermore, after 5 turns the position of the minimum hardness is displaced from the disc centre for the smooth anvil, but it remains essentially in the centre position for the rough anvil.

A comparison of hardness evolution on the bottom surfaces with smooth and rough anvils

To compare the influence of smooth and rough anvils on the mechanical characteristics for the disc bottom surfaces,

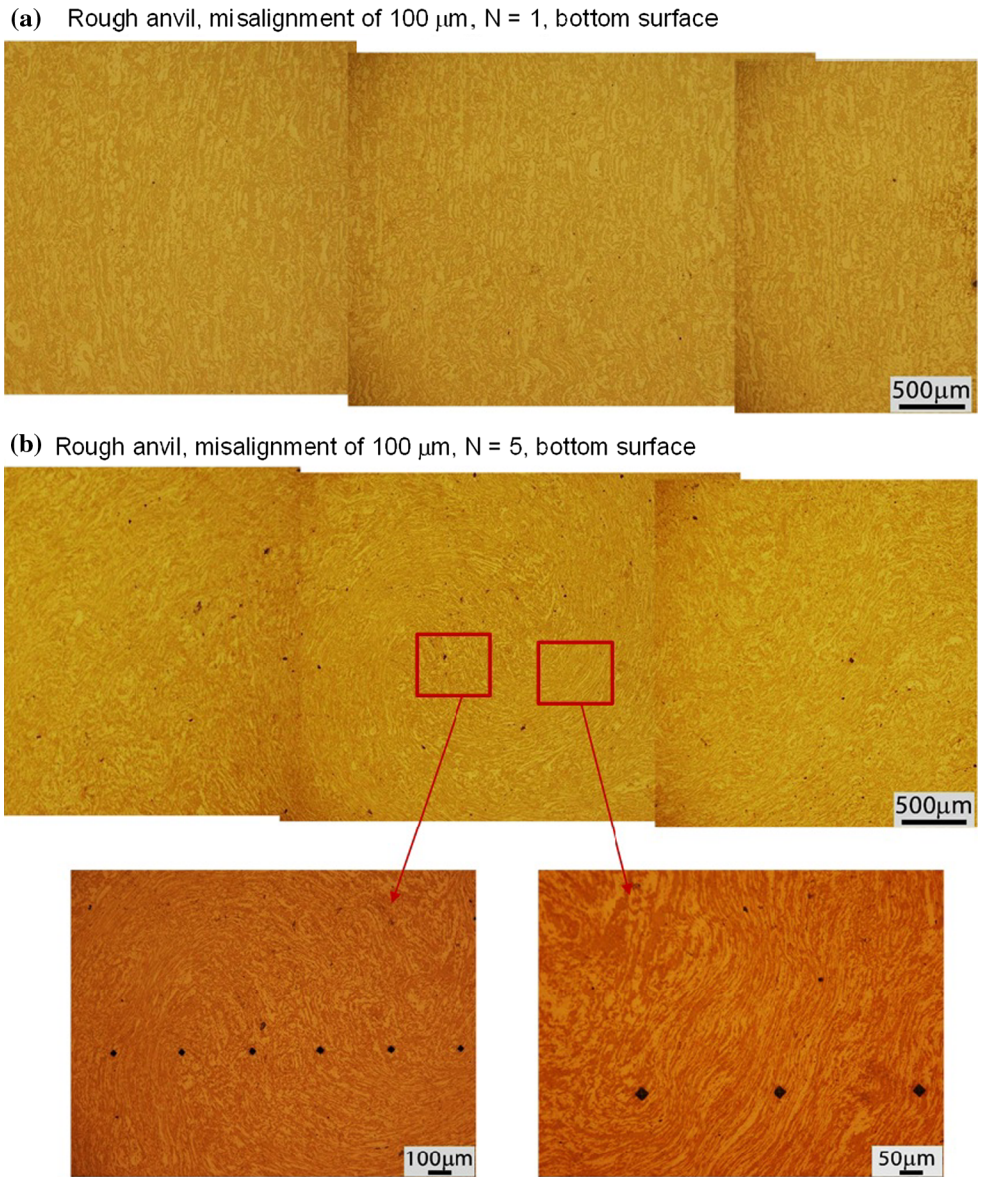

Fig. 6 The flow pattern appearance on the disc bottom surface while using rough anvils ($R_a = 15$ μm) with an anvil misalignment of 100 μm for **a** $N = 1$ turn and **b** $N = 5$ turns

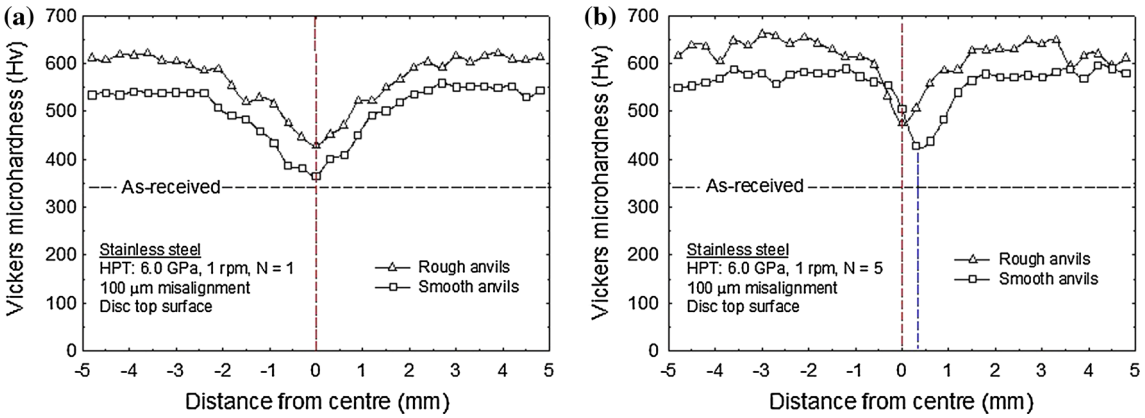

Fig. 7 Hardness distributions on the disc top surface after **a** 1 and **b** 5 turns using smooth and rough anvils

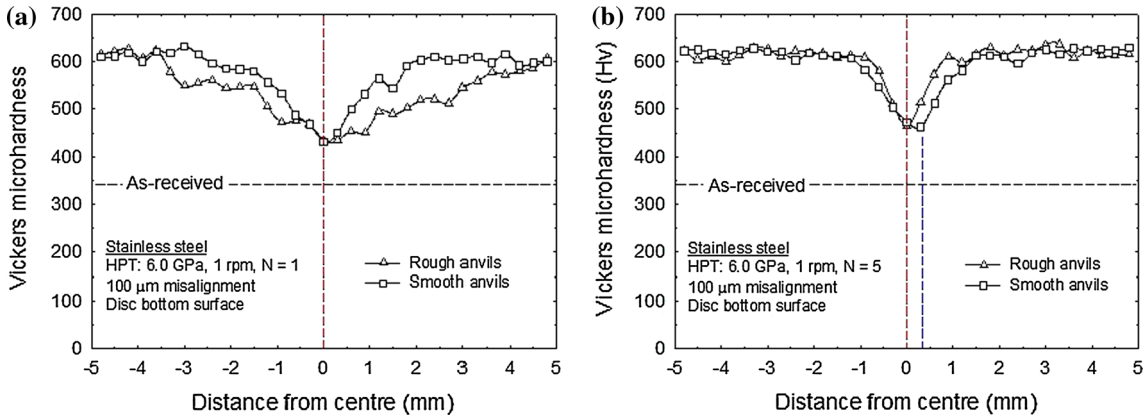

Fig. 8 Hardness distributions on the disc bottom surface after **a** 1 and **b** 5 turns using smooth and rough anvils

hardness distributions were recorded on the bottom surfaces as shown in Fig. 8 after (a) 1 and (b) 5 turns.

After 1 turn, double-swirl flow patterns are visible on the bottom surfaces with the smooth anvil, whereas the phase domains have a straight appearance with the rough anvil. Due to these different flow patterns, the hardness distributions for the smooth and rough anvils have different variations. As shown in Fig. 8 (a), with the smooth anvil the hardness distribution displays a two-stage behaviour which includes an initial linear variation between hardness and distance around the centre of the disc and then a saturation plateau. With rough anvils, the hardness values increase almost linearly with the disc radius from the centre to the edge. The linear variations of hardness on the bottom surface with the rough anvil demonstrate that the shear strain at the disc bottom is very close to the ideal rigid-body assumption. Overall, the hardness values at the bottom surface tend to be larger with the smooth anvil than with the rough anvil.

After 5 turns, smooth anvils produce double-swirl flown patterns on the disc bottom surface, whereas rough anvils generate the appearance of a single swirl with a non-uniform phase domain contrast. Figure 8 (b) shows the overall microhardness values at the disc bottom surface using the rough and smooth anvils. In Fig. 8 (b), both sets of data have similar values after processing through 5 turns of rotation, but for the smooth anvil; the minimum hardness position is again displaced from the centre position while the minimum hardness remains at the centre for the rough anvil.

Discussion

Comparing the surface morphology images of the depressions within the smooth and rough anvils in Fig. 2, it is readily apparent that the smooth anvil has not only a smaller value of R_a but also a smaller area for each pit. Overall, the smooth anvil surface in Fig. 2 (a) has shallow pits and a reasonably uniform pit distribution, whereas the rough anvil surface in Fig. 2 (b) has deeper and larger pits with a fairly non-uniform distribution. During HPT processing, the hydrostatic pressure which is imposed initially leads to a plastic flow of the sample material into the micro-asperities on the anvil surfaces within the depressions, and this provides an excellent fit between the sample and the anvil for subsequent rotational straining. Thus, shear deformation occurs in the interior of the disc sample.

With the rough anvil, the pit area and pit depth are large and the pit distribution is non-uniform so that the local frictional forces change from place to place during the HPT processing. These variations in the local frictional forces affect the flow patterns of the deformed materials. With the smooth anvil, the pit area and pit depth are relatively small and the pit distribution is reasonably uniform so that the local frictional force is reasonably uniform from place to place during the HPT processing. Due to the different surface roughness characteristics of the smooth and rough anvils, it is readily apparent that samples processed to the same numbers of rotations will have different flow patterns and hardness distributions depending on the precise nature of the anvil surfaces. Both the flow patterns and the refinement in width of the austenitic (γ) and the ferritic (α) phases make contributions to the hardness distributions on the top and bottom surfaces of the disc.

After 1 turn of rotation on the disc top surface, there are clear double-swirl flow patterns on samples processed with the smooth anvil, whereas the double-swirls are less easy to identify on the sample processed using the rough anvil. It is important to define and make a meaningful distinction between the terms *clear double-swirl flow patterns* and *recognisable double-swirl flow patterns*. The former have smooth and well-defined phase domains in low magnification images as shown in Fig. 3 (a) whereas the latter have

many local vortices and locally there is significantly refined austenitic γ and ferritic α phases as shown in Fig. 5 (a). It is reasonable to assume that variations in the local frictional forces introduced by the rough anvil contribute to the so-called recognisable double-swirl flow patterns. Furthermore, although the disc top surface shows a double-swirl flow pattern after 1 turn when using smooth or rough anvils, because of the obvious refinement in the widths of the austenitic γ and ferritic α phases with the rough anvil, as shown in Fig. 7 (a), the sample processed by 1 turn on the rough anvil has higher hardness values on the disc top surface than for the smooth anvil.

After 5 turns of rotation on the disc bottom surface, there are clear double-swirl flow patterns but with a smaller configuration when using the smooth anvil, whereas there is a single swirl flow pattern on the sample processed using the rough anvil. The double-swirl flow pattern has smooth and well-defined phase domains in the low magnification image shown in Fig. 4 (b), whereas the single swirl has local vortices in the swirl centre area and local austenitic γ and ferritic α phases which are significantly refined as shown in Fig. 6 (b). It is reasonable to assume that the local friction force variation introduced by the rough anvil leads to the single swirl flow pattern. With the smooth anvil, the disc bottom surface has double-swirl flow patterns, whereas with the rough anvil a single-swirl flow pattern accompanied by a refinement in the width of the austenitic (γ) and the ferritic (α) phases appears on the bottom surface. It is assumed the hardness value should be higher when using a rough anvil than when using a smooth anvil on the disc bottom surface but, as shown in Fig. 8 (b), the disc bottom surface of the sample processed by 5 turns with the rough anvil has similar hardness values as with the sample processed by the smooth anvil. Thus, the difference in flow patterns on the disc bottom surface failed to make a major contribution to the hardness values after 5 turns.

It should be noted that in the as-received stainless steel the widths of the austenitic (γ) and the ferritic (α) phases do not have a uniform size distribution, as shown in Fig. 1, but instead the widths vary from ~5 to ~50 μm. When using smooth anvils, *clear double-swirl flow patterns* and well-defined phase domains are present on the top and bottom surface and there are no significant refinements in the widths of the austenitic (γ) and the ferritic (α) phases. When using rough anvils, after 1 turn the disc top surface shows *a recognizable double-swirl flow pattern* with local refined austenitic (γ) and ferritic (α) phases. After 5 turns, the disc top and bottom surfaces show single-swirl flow patterns with local significantly refined austenitic (γ) and ferritic (α) phases. In these local refined phase domain areas, the measured widths of the austenitic (γ) and the ferritic (α) phases vary between ~1 and ~20 μm after 1 and 5 turns, where these values are significantly refined by comparison with the range from ~5 to ~50 μm for the austenitic (γ) and ferritic (α) phases in the as-received condition.

Finally, it is important to note that, although the strain varies significantly across the discs in HPT processing as documented in Eq. (1), there is a gradual evolution towards microstructural homogeneity with increasing numbers of revolutions and this evolution has been reported experimentally [22, 36–42] and predicted theoretically using strain gradient plasticity modelling [19].

Summary and conclusions

[1] Experiments were undertaken using a super duplex stainless steel to evaluate the influence of anvil surface roughness on the flow patterns and hardness evolution on the disc top and bottom surfaces using a fixed anvil misalignment of 100 μm during HPT processing. The experiments were conducted using smooth and rough anvils with roughness values of $R_a = 5$ μm and $R_a = 15$ μm, respectively.

[2] The results show that the same double-swirl flow patterns develop on the disc top and bottom surfaces when using a smooth anvil and the double-swirl configuration decreases with increasing numbers of rotations. When using a rough anvil, the disc top and bottom surfaces have the same single swirl flow patterns for 5 turns, whereas for 1 turn the disc top surface has a recognisable double-swirl flow pattern and the disc bottom surface has straight phase domains.

[3] While using rough anvils, there are two common features in the disc surface flow patterns. First, there are non-uniform phase domains with some areas having significantly refined austenitic γ and ferritic α phases. Second, there are some areas having local vortices. These features are attributed to variations in the local frictional forces which cause unstable flow and non-uniform structural refinement.

[4] Due to the local refinement of the austenitic γ and ferritic α phases when using the rough anvil, the disc top surface has larger hardness values than when using a smooth anvil. By contrast, there are no significant hardness differences at the bottom surface when using rough and smooth anvils.

Acknowledgements The authors thank Dr Liam Goodes for assistance during the anvil surface roughness measurements. This work was supported by the European Research Council under ERC Grant Agreement No. 267464-SPDMETALS.

References

1. Zhilyaev AP, Langdon TG (2008) Using high-pressure torsion for metal processing: fundamentals and applications. Prog Mater Sci 53:893–979
2. Kawasaki M, Figueiredo RB, Langdon TG (2012) Twenty-five years of severe plastic deformation: recent developments in evaluating the degree of homogeneity through the thickness of disks processed by high-pressure torsion. J Mater Sci 47:7719–7725. doi:10.1007/s10853-012-6507-y
3. Korznikov AV, Safarov IM, Laptionok DV, Valiev RZ (1991) Structure and properties of superfine-grained iron compacted out of ultradisperse powder. Acta Metall Mater 39:3193–3197
4. Edalati K, Horita Z, Fujiwara H, Ameyama K (2010) Cold consolidation of ball-milled titanium powders using high-pressure torsion. Metall Mater Trans A 41A:3308–3317
5. Zhilyaev AP, Gimazov AA, Raab GI, Langdon TG (2008) Using high-pressure torsion for the cold-consolidation of copper chips produced by machining. Mater Sci Eng, A 486:123–126
6. Miyazaki T, Terada D, Miyajima Y, Suryanarayana C, Murao R, Yokoyama Y, Sugiyama K, Umemoto M, Todaka Y, Tsuji N (2011) Synthesis of non-equilibrium phases in immiscible metals mechanically mixed by high pressure torsion. J Mater Sci 46:4296–4301. doi:10.1007/s10853-010-5240-7
7. Waitz T, Kazykhanov V, Karnthaler HP (2004) Martensitic phase transformations in nanocrystalline NiTi studied by TEM. Acta Mater 52:137–147
8. Révész Á, Hóbor S, Lábár JL, Zhilyaev AP, Kovács Z (2006) Partial amorphization of a Cu–Zr–Ti alloy by high pressure torsion. J Appl Phys 100:103522 (1–7)
9. Ivanisenko Y, Kilmametov A, Rösner H, Valiev RZ (2008) Evidence of alpha → omega phase transition in titanium after high pressure torsion. Int J Mater Res 99:36–41
10. Pérez-Prado MT, Zhilyaev AP (2009) First experimental observation of shear induced hcp to bcc transformation in pure Zr. Phys Rev Lett 102:175504 (1–4)
11. Wang YB, Zhao YH, Lian Q, Liao XZ, Valiev RZ, Ringer SP, Zhu YT, Lavernia EJ (2010) Grain size and reversible beta-to-omega phase transformation in a Ti alloy. Scr Mater 63:613–616
12. Leiva DR, Jorge AM, Ishikawa TT, Huot J, Fruchart D, Miraglia S, Kiminami CS, Botta WJ (2010) Nanoscale grain refinement and H-sorption properties of MgH_2 processed by high-pressure torsion and other mechanical routes. Adv Eng Mater 12:786–792
13. Edalati K, Yamamoto A, Horita Z, Ishihara T (2011) High-pressure torsion of pure magnesium: evolution of mechanical properties, microstructures and hydrogen storage capacity with equivalent strain. Scr Mater 64:880–883
14. Wang XD, Cao QP, Jiang JZ, Franz H, Schroers J, Valiev RZ, Ivanisenko Y, Gleiter H, Fecht H-J (2011) Atomic-level structural modifications induced by severe plastic shear deformation in bulk metallic glasses. Scr Mater 64:81–84
15. Wang YB, Qu DD, Wang XH, Cao Y, Liao XZ, Kawasaki M, Ringer SP, Shan ZW, Langdon TG, Shen J (2012) Introducing a strain-hardening capability to improve the ductility of bulk metallic glasses via severe plastic deformation. Acta Mater 60:253–260
16. Valiev RZ, Ivanisenko YuV, Rauch EF, Baudelet B (1996) Structure and deformation behaviour of Armco iron subjected to severe plastic deformation. Acta Mater 44:4705–4712
17. Figueiredo RB, Cetlin PR, Langdon TG (2011) Using finite element modeling to examine the flow processes in quasi-constrained high-pressure torsion. Mater Sci Eng, A 528:8198–8204
18. Figueiredo RB, Pereira PHR, Aguilar MTP, Cetlin PR, Langdon TG (2012) Using finite element modeling to examine the temperature distribution in quasi-constrained high-pressure torsion. Acta Mater 60:3190–3198
19. Estrin Y, Molotnikov A, Davies CHJ, Lapovok R (2008) Strain gradient plasticity modelling of high-pressure torsion. J Mech Phys Solids 56:1186–1202
20. Xu C, Horita Z, Langdon TG (2007) The evolution of homogeneity in processing by high-pressure torsion. Acta Mater 55:203–212
21. Wongsa-Ngam J, Kawasaki M, Zhao Y, Langdon TG (2011) Microstructural evolution and mechanical properties of a Cu–Zr alloy processed by high-pressure torsion. Mater Sci Eng, A 528:7715–7722
22. Kawasaki M, Figueiredo RB, Langdon TG (2011) An investigation of hardness homogeneity throughout disks processed by high-pressure torsion. Acta Mater 59:308–316
23. Loucif A, Figueiredo RB, Baudin T, Brisset F, Chemam R, Langdon TG (2012) Ultrafine grains and the Hall-Petch relationship in an Al–Mg–Si alloy processed by high-pressure torsion. Mater Sci Eng, A 532:139–145
24. Wongsa-Ngam J, Kawasaki M, Langdon TG (2012) Achieving homogeneity in a Cu–Zr alloy processed by high-pressure torsion. J Mater Sci 47:7782–7788. doi:10.1007/s10853-012-6587-8
25. Sabbaghianrad S, Kawasaki M, Langdon TG (2012) Microstructural evolution and the mechanical properties of an aluminum alloy processed by high-pressure torsion. J Mater Sci 47:7789–7795. doi:10.1007/s10853-012-6524-x
26. Cao Y, Wang YB, Alhajeri SN, Liao XZ, Zheng WL, Ringer SP, Langdon TG, Zhu YT (2010) A visualization of shear strain in processing by high-pressure torsion. J Mater Sci 45:765–770. doi:10.1007/s10853-009-3998-2
27. Cao Y, Kawasaki M, Wang YB, Alhajeri SN, Liao XZ, Zheng WL, Ringer SP, Zhu YT, Langdon TG (2010) Unusual macroscopic shearing patterns observed in metals processed by high-pressure torsion. J Mater Sci 45:4545–4553. doi:10.1007/s10853-010-4485-5
28. Cao Y, Wang YB, Figueiredo RB, Chang L, Liao XZ, Kawasaki M, Zheng WL, Ringer SP, Langdon TG, Zhu YT (2011) Three-dimensional shear-strain patterns induced by high-pressure torsion and their impact on hardness evolution. Acta Mater 59:3903–3914
29. Tian YZ, An XH, Wu SD, Zhang ZF, Figueiredo RB, Gao N, Langdon TG (2010) Direct observations of microstructural evolution in a two-phase Cu-Ag alloy processed by high-pressure torsion. Scr Mater 63:65–68
30. Vorhauer A, Pippan R (2004) On the homogeneity of deformation by high pressure torsion. Scr Mater 51:921–925
31. Hohenwarter A, Bachmaier A, Gludovatz B, Scheriau S, Pippan R (2009) Technical parameters affecting grain refinement by high pressure torsion. Int J Mater Res 100:1653–1661
32. Huang Y, Kawasaki M, Langdon TG (2013) An investigation of flow patterns and hardness distributions using different anvil alignments in high-pressure torsion. J Mater Sci 48:4533–4542. doi:10.1007/s10853-012-7015-9
33. Huang Y, Kawasaki M, Langdon TG (2013) Influence of anvil alignment on shearing patterns in high-pressure torsion. Adv Eng Mater 15:747–755
34. Huang Y, Kawasaki M, Langdon TG (2014) An evaluation of the shearing patterns introduced by different anvil alignments in high-pressure torsion. J Mater Sci 49:3146–3157. doi:10.1007/s10853-014-8015-8
35. Edalati K, Horita Z, Langdon TG (2009) The significance of slippage in processing by high-pressure torsion. Scr Mater 60:9–12
36. Zhilyaev AP, Lee S, Nurislamova GV, Valiev RZ, Langdon TG (2001) Microhardness and microstructural evolution in pure nickel during high-pressure torsion. Scr Mater 44:2753–2758
37. Zhilyaev AP, Nurislamova GV, Kim BK, Baró MD, Szpunar JA, Langdon TG (2003) Experimental parameters influencing grain

refinement and microstructural evolution during high-pressure torsion. Acta Mater 51:753–765
38. An XH, Wu SD, Zhang ZF, Figueiredo RB, Gao N, Langdon TG (2010) Evolution of microstructural homogeneity in copper processed by high-pressure torsion. Scr Mater 63:560–563
39. An XH, Lin QY, Wu SD, Zhang ZF, Figueiredo RB, Gao N, Langdon TG (2011) The influence of stacking fault energy on the mechanical properties of nanostructured Cu and Cu-Al alloys processed by high-pressure torsion. Scr Mater 64:954–957
40. An XH, Lin QY, Wu SD, Zhang ZF, Figueiredo RB, Gao N, Langdon TG (2011) Significance of stacking fault energy on microstructural evolution in Cu and Cu-Al alloys processed by high-pressure torsion. Philos Mag 91:3307–3326
41. Langdon TG (2013) Twenty-five years of ultrafine-grained materials: achieving exceptional properties through grain refinement. Acta Mater 61:7035–7059
42. Kawasaki M (2014) Different models of hardness evolution in ultrafine-grained materials processed by high-pressure torsion. J Mater Sci 49:18–34. doi:10.1007/s10853-013-7687-9